Smart Structures and Systems, *Vol. 17, No. 1 (2016) 17-29*
DOI: http://dx.doi.org/10.12989/sss.2016.17.1.017

Air-coupled ultrasonic tomography of solids: 1 Fundamental development

Kerry S. Hall*[1] and John S. Popovics[2a]

[1]*Department of Engineering, University of Southern Indiana, 8600 University Blvd, Evansville, IN 47712, USA*
[2]*Department of Civil and Environmental Engineering, University of Illinois at Urbana-Champaign, 205 N Mathews Ave, Urbana, IL 61801, USA*

(Received February 12, 2014, Revised September 19, 2014, Accepted October 29, 2014)

Abstract. Ultrasonic tomography is a powerful tool for identifying defects within an object or structure. But practical application of ultrasonic tomography to solids is often limited by time consuming transducer coupling. Air-coupled ultrasonic measurements may eliminate the coupling problem and allow for more rapid data collection and tomographic image construction. This research aims to integrate recent developments in air-coupled ultrasonic measurements with current tomography reconstruction routines to improve testing capability. The goal is to identify low velocity inclusions (air-filled voids and notches) within solids using constructed velocity images. Finite element analysis is used to simulate the experiment in order to determine efficient data collection schemes. Comparable air-coupled ultrasonic signals are then collected through homogeneous and isotropic solid (PVC polymer) samples. Volumetric (void) and planar (notch) inclusions within the samples are identified in the constructed velocity tomograms for a variety of transducer configurations. Although there is some distortion of the inclusions, the experimentally obtained tomograms accurately indicate their size and location. Reconstruction error values, defined as misidentification of the inclusion size and position, were in the range of 1.5-1.7%. Part 2 of this paper set will describe the application of this imaging technique to concrete that contains inclusions.

Keywords: non-destructive testing; ultrasound; tomography; non-contact; air-coupled

1. Introduction

Ultrasonic tomography is a powerful tool for identifying defects within an object or structure, providing the ability to image internal sections throughout solid structural elements. This method can be applied on structures where x-ray tomography is impractical due to size, low contrast, or safety concerns. Using ultrasonic measurements taken through the object, images of internal velocity or attenuation variations can be re-constructed. However, many ultrasonic data projections must be collected across the entire imaged area (Koduru and Rose 2013) or through the volume (Abbaszadeh *et al*. 2013) in order to re-construct images with high resolution and accuracy. This need for a high density of data projections normally requires multiple-unit ultrasonic transducer arrays to be mounted directly on the tested surface. This testing configuration and data collection

∗Corresponding author, Assistant Professor, E-mail: khall@usi.edu
[a] Professor, Email: johnpop@illinois.edu

http://www.techno-press.org/?journal=sss&subpage=8 ISSN: 1738-1584 (Print), 1738-1991 (Online)

process are time consuming because of the need for surface preparation and coupling. As a result there is broad interest in using contactless transducers to make more rapid ultrasonic measurements through solids. These methods eliminate the need for surface preparation, couplants, and errors associated with variable sensor application pressure.

Contactless ultrasonic measurements are made possible by air-coupled (acoustic) transducers, lasers, or, for conducting materials, electro-magnetic acoustic transducers (EMATs). Air-coupled ultrasonic transducers offer the broadest range of application as they are relatively insensitive to material surface roughness conditions (unlike lasers) and can be applied to all solid materials (unlike EMATs). Because surface preparation is a limiting step in the speed of data collection, air-coupled ultrasonic tests would allow for the collection of more ultrasonic data on a specimen under time restrictions, allowing for automated and rapid collection of data for tomography. However, the large acoustic impedance difference brings a large reduction of transmitted energy at the interface of air and the solid material. Additional material attenuation (scattering and viscous losses) of ultrasonic waves traveling through solid material adds to this problem. Nonetheless, special testing configurations and signal processing methods have been applied to overcome these challenges. Dhital and Lee (2012) used a hybrid (laser and air-coupled transducer) one-sided testing configuration to image surface cracks in aluminum plates. Using non-contact ultrasonic transmission measurements with capacitive transducers, Berriman *et al*. (2005) tested the effects of humidity and aggregate content in 25 mm thick concrete plates and Sanabria *et al*. (2011) tested glue bonding in 10 mm thick glued timber specimens. Air-coupled ultrasonic data have also been used to create tomograms of solid elements (Ho *et al*. 2007, Gan *et al*. 2002). In these tomographic studies, large amounts of data are collected efficiently, but these applications were limited to thin-walled metal vessels that were filled with water (simulating food and beverage containers), where metal bars were located within the water using attenuation tomography. These samples do not provide extensive wave paths through lossy solid materials, and furthermore applications were also relatively small in scale: the largest container imaged was only 66 mm in diameter. Further investigation is necessary to overcome significant experimental issues associated with air-coupled ultrasonic tomography of extensive solid elements, such as spectral reflection, mode conversion, material scattering and loss, and interference effects. We consider these issues and explore the viability of fully air-coupled ultrasonic tomography for solids in this paper, with the ultimate aim of extending the application of air-coupled ultrasonic tomography to defect detection in structural elements.

2. Background information and previous work

2.1 Ultrasonic velocity measurements

Ultrasonic P-wave pulse velocity (UPV) measurements are often used in the tomography of solids. One advantage of UPV is that by using only first arrival of the P-wave, confusion of multiple reflections within the specimen is avoided (Naik *et al*. 2004). Unfortunately the amplitude of this first arrival is small compared to the peak amplitude of an ultrasonic pulse. In order to overcome this limitation, the signal to noise ratio (SNR) must be optimized by using special transducers and processing.

UPV measurements are typically made using piezoelectric transducers. These transducers use a crystal tuned to the frequency of interest to convert voltage into displacements for transmission.

These transducers are typically designed for transmission into solids and transmit poorly into air owing to the very large acoustic impedance mismatch between air and the crystal material. Some researchers have improved transmission through air by adding a matching layer on the transducer face. This matching layer provides a transition impedance, and the thickness is controlled to set up a resonance with the frequency being transmitted (Cetrangalo and Popovics 2010). Others have incorporated low impedance materials into piezoelectric composites to reduce the impedance mismatch with air and increase the transmitted and received energy (Wright *et al*. 1996). Researchers have also looked for alternatives to piezoelectric transducers. Capacitive transducers, also known as electrostatic transducers, use the potential difference between a plate and a vibrating membrane to drive the mechanical generation of ultrasonic waves in air. Capacitive transducers can also detect pressure differences with high sensitivity and over a broad bandwidth of frequencies (Berriman *et al*. 2005). Capacitive transducers were chosen for this research because they can produce higher amplitude pulses in air and offer a higher degree of control of pulse duration compared to piezoelectric transducers.

To further improve the SNR in air coupled measurements, signal processing is employed. Time averaging is often used if the speed of data collection is not critical. Time averaging is simply the process of collecting many signals under the same conditions and adding them together to reduce incoherent signal content. Weighted moving averages can also be used to remove high frequency noise without distorting a signal. Although moving averages do not provide a sharp frequency cutoff, they also do not add ripples in the time domain signal that can occur with spectral processes such as digital filtering. The number of points averaged around each point determines the frequency of the filter. With broad frequency bandwidth transducers, pulse compression also can be applied to improve SNR. This method typically utilizes frequency and amplitude modulated excitation signals. A reference signal is cross-correlated to the signal transmitted through the specimen in order to accurately determine the arrival time with improved SNR (Berriman *et al.* 2005). When narrow frequency bandwidth excitation pulses are used, wavelet analysis can be a powerful tool to reduce noise levels. By correlating single frequency wavelets over the signal and summing the resulting coefficients, a narrowly filtered signal (small frequency passband) can be produced (Cetrangalo and Popovics 2010).

Although all of the above-listed processing methods are reported to improve signals, we found that time averaging and a triangular weighted moving average were sufficient for our data. In particular we did not use spectral methods or pulse compressions in order to avoid distortion and ripples in the time domain signals, which can cause false arrival indications for UPV measurements. The resulting processed UPV data were input to the tomographic reconstruction algorithm.

2.2 Tomographic imaging

Tomography is the production of cross-sectional images of an object using information from projections through the object. The projections used in conventional tomography are velocity or attenuation measurements of ultrasonic or electromagnetic pulses transmitted through the object. Radon proved that an image of a cross-section could be reconstructed perfectly given a complete set of projections through the section (Radon 1917). Unfortunately an ideal, complete set of measurements often cannot be obtained for many ultrasonic applications for solids, for example because of geometric and material constraints (Jackson and Tweeton 1994). When geometric constraints limit measurements, series expansion techniques can be used to approximate the field

of slowness (inverse of the velocity field) or attenuation. The slowness field can be calculated by multiplying the time of flight of the waves by the inverse of the matrix of distance traveled through each pixel by each wave. The ideal sensors configuration for Radon's tomography is an arc of receivers equidistant from the transmitters. When this configuration is not possible, or when the inversion of the distance matrix is not practical, an Algebraic Reconstruction Technique (ART) is implemented to approximate the solution (Jackson and Tweeton 1994).

The ART is an iterative algorithm. First, a vector of the time of flight measurements, **T**, is input to the model with accompanying coordinates of the source and receiver positions. The expected average velocity of the material is used as a uniform initial velocity field. Each element of the velocity field vector is inverted to calculate the slowness field vector, **P**, which has a length equal to the number of pixels in the field. The initial estimate of slowness field for the current iteration is denoted as P_0. The ray paths can either be assumed to be straight or determined by hybrid bending. If bent rays are used, the ray paths can be recalculated at each iteration for P_0. The lengths of each of the ray paths that pass through each pixel is stored in the matrix **D**, which has rows representing each pixel in the field and columns representing each ray path measurement that was input to the model. The vector of the times of flight, $\mathbf{T_0}$, along the paths of the current iteration is then computed by

$$\mathbf{T_0} = \mathbf{D}P_0 \tag{1}$$

The residual error from the actual time of flight measurements, dT_0, is then calculated and the incremental change to the slowness field, dP_0, is back-projected using a row-normalized transpose of the matrix **D**

$$dP_0 = \mathbf{D}^T dT_0 \tag{2}$$

The slowness field for the next iteration can then be calculated. This process is repeated until the increment, dP_0, becomes suitably small compared to the average value of the slowness field.

3. Experimental setup

3.1 Signals

An air-coupled transmission system was developed to measure the first arrivals in an automated process. The goal of the system was to make rapid and accurate UPV measurements through poly-vinyl chloride (PVC) polymer test samples. A short pulse with a central frequency of 50 kHz was selected as the transmission signal. Capacative transducers (Senscomp 600) with a center frequency of approximately 50 kHz were used. Fig. 1 shows the short pulse time signal collected along a short direct path through air; the frequency content of the pulse shows a distribution of frequencies centered about 52 kHz. All short pulse signals were collected after 1000 time averages to improve SNR for non-contact transmission. The data were digitized with a sampling rate of 10 MHz and then sent to a computer for subsequent analysis. A triangular moving average was used to filter out high frequency noise without significantly disturbing the first arrival indication for the central frequency of 52 kHz. The first arrival of the pulse in the time signal is determined using an amplitude threshold, where the time that the signal first exceeds the assigned threshold is identified. The amplitude of the threshold is set just above the general noise level, and is determined for each set of signals collected. An example non-contact transmission time signal,

collected through a PVC cylinder, is shown in Fig. 2 before and after processing. In this signal the threshold amplitude is 0.01 mV.

Non-contact UPV was then implemented to image various inclusions within 152 mm (6 inch) diameter PVC cylinders.

3.2 PVC specimens

After a developing a tomographic reconstruction algorithm and air-coupled measurement system, a set of specimens were fabricated to evaluate the system. PVC was selected for the phantoms because of its lower acoustic impedance which reduces the transmission losses into and out of air. PVC represents a homogeneous isotropic solid at the scale of the ultrasonic wavelength employed in these tests. However the attenuation of ultrasound in PVC is not negligible and is absorptive rather than scattering in nature. Two cylindrical phantoms 152 mm in diameter were prepared with different inclusions, as shown in Fig. 3.

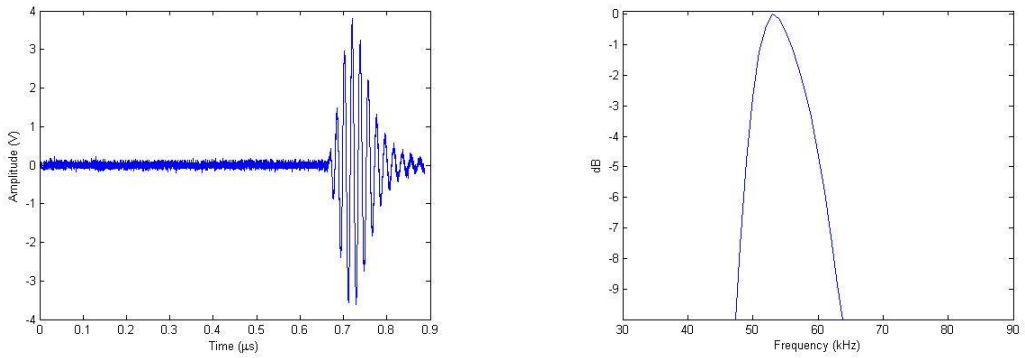

Fig. 1 Reference signal through air: (left) raw time signal and (right) spectral (amplitude) representation of signal

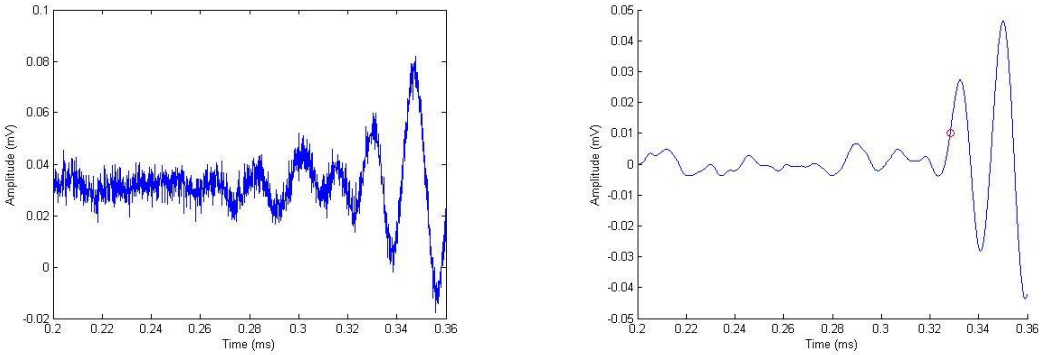

Fig. 2 Fully air-coupled transmission through PVC cylinder: (left) raw time signal and (right) time signal after time averaging and weighted moving average filtering (red circle indicates first arrival)

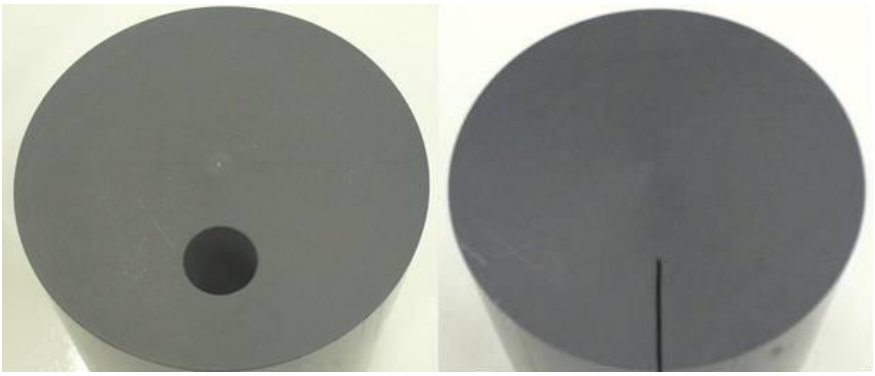

Fig. 3 PVC cylinder samples: (left) 25 mm diameter void sample and (right) crack sample. Both samples have a cross-sectional diameter of 152 mm

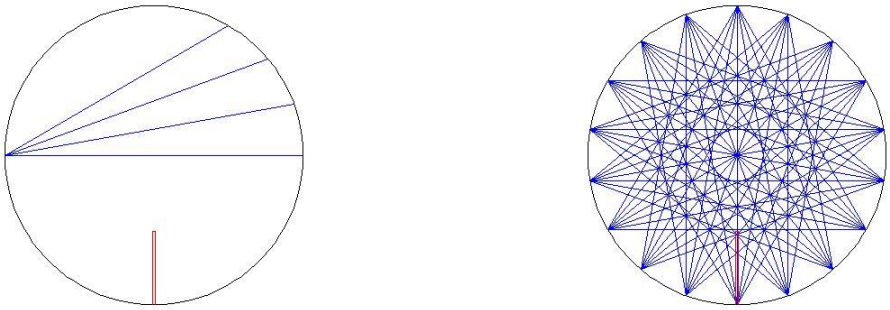

Fig. 4 Ray paths of a single experimental testing position for 45^{o} fan width (left) and complete ray coverage for 15^{o} transducer spacing (right)

The inclusions are uniform through the length of the specimens so that the problem can be considered to be two-dimensional when we image a central cross-sectional slice through the sample. The circular void is 25 mm in diameter and located 38 mm radially from the center. The notch was cut 38 mm radially into the side of the specimen and is approximately 1 mm wide. These defects represent disparate defect conditions with regard to shape, size and internal position.

3.3 Measurement patterns (Ray Coverage)

The arrangement of measurement paths through a cross-section is important in producing good tomograms, especially to detect internal defects. Thus, ray coverage patterns were carefully selected to be appropriate for the two disparate defect conditions in the PVC sample. For this study ultrasonic waves are sent and received along multiple intersecting wave paths that lie on a single plane that is normal to the central axis of the cylinder. The ray paths for the cylindrical specimens in this work are described with respect to the center of the cylinder cross-section, assuming that

the specimen is fixed in position and surrounded by transducers.

The angle of offset from direct transmission is measured with reference to the center of the cylinder, and the maximum angle of offset for a data set will be referred to as the fan width. Because only one transmitter and receiver were used for data collection, the fan width was controlled by rotating the position of the transmitter circumferentially about the specimen while the receiver remained stationary. The transducer spacing will be the angle between measurement points on the surface with reference to the center of the cylinder. The transducer spacing was actually controlled by rotating the specimen while the transmitter and receiver remained stationary. Fig. 4 illustrates ray coverage with a 45° fan width and 15° transducer spacing. To evaluate whether these ray path measurement patterns would be sufficient to detect the inclusions, a finite element model was used to simulate many path configurations.

4. Finite element model

Finite element models of these specimens were developed in order to understand more clearly the effect of different inclusion types and the measurement ray patterns on the ultrasonic signals. The models were also useful for comparing different measurement configurations. Large sets of simulated ultrasonic time signal data were generated quickly with these models and then reduced to various limited data sets to evaluate the effect of ray coverage density and ray distribution on the quality of tomographic reconstructions. Ray coverage density is quantified by dividing the number of rays by the cross-sectional area of the specimen.

The ABAQUS software platform was used to perform the dynamic finite element analyses. The cross-section of the specimens was represented in 2-D plane strain. The plane strain assumption prescribes the specimen to be continuous and uniform out of plane, which is appropriate for this case as we are only interested in the first arrival of the ultrasonic waves for pulse velocity measurements within a given cross-sectional slice through the specimen. The only significant error introduced by this assumption is that the simulated signal amplitudes will be somewhat higher without geometric dispersion of the wave energy out of plane.

The mesh was made up of 4-node bilinear elements with a nominal size of 1mm. The analysis was executed with an explicit formulation with no boundary conditions and a maximum time step of 0.4 μs. Transient displacement loading, applied in the direction normal to the surface at one point (mesh node) on the surface, had the form of a single cycle of 50 kHz sine function. This loading function simulates the mechanical excitation of the surface by the ultrasonic transmitter. Although this excitation form does not perfectly represent the case of a surface insonified by an air-coupled transducer with limited frequency content, the simulation does allow insight to the complicated internal wave propagation and defect interaction. A short one-cycle excitation was applied here in order to maximize axial resolution so that these reflections, refractions and mode conversion of the signal could be clearly distinguished. The base material properties of the cylinder were set to match the properties of the PVC specimens so that the P-wave velocity in the model would match the known 2520 m/s velocity of the PVC. For further information on the details of the model, refer to Hall (2011.)

Three 25 mm diameter inclusions were incorporated into the model individually as separate components. These components were positioned 25, 38, and 51 mm from the center of the cylinder and 120° apart from each other circumferentially, as shown in Fig. 5. By changing the material assigned to these components, specimens with various inclusions could be simulated. The

component positioned 38 mm from the center simulates the PVC void sample used in the experiments; the other void positions were included to observe the effects of defect position for other studies beyond the scope of this paper. In this study, the air-filled inclusion was simulated by deleting the elements within the circular component located 38 mm from the center (blue circle in Fig. 5), while the stiffness and density properties of the other two (red and yellow) inclusions were set to match the properties of the rest of the model. This mesh configuration allows testing of different void locations with the same mesh, providing computational efficiency. In order to simulate the PVC notch sample, all circular inclusions were set to match the base material and one row of elements along the centerline was removed to a depth of 38 mm from the outer edge.

5. Tomographic simulations

Transient displacement signals were recorded around the surface of the cylinder at points where receivers would be positioned to achieve 5° transducer spacing and a maximum fan width of 90°. Signals were recorded with a sampling interval of 0.1 μs and 10 ms duration. These simulated transmitters and receivers were rotated about the specimen in a series of 72 finite element analyses to achieve the desired ray coverage patterns described below. These signals were processed as UPV measurements to generate the simulation datasets. The known P-wave velocity of PVC, 2520 m/s, was used as the initial guess for the velocity field reconstruction.

The geometry of our testing configuration does not match the ideal case for Radon transform because our receivers are approximated on the surface of the circle. Thus ART was used to reconstruct tomograms from the dataset. In order to compare tomograms quantitatively, an imaging error was calculated for each tomogram. In the reconstructed image, defect (void) areas were identified by pixels with velocity values within the lowest 25% of the complete velocity population in the tomogram. The 25% threshold was chosen after trial and error study using a range of experimental tomographic data sets from samples with known defects. The 25% threshold level provides tomograms that describe the location of defects with optimal accuracy. Defect pixels were then assigned a value of 0 and solid material was assigned a value of 1. The image error was calculated as the difference between the predicted defects of a tomogram and the actual prescribed defect in the finite element model, computed pixel by pixel.

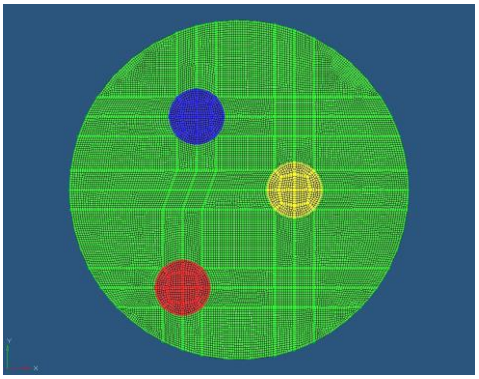

Fig. 5 Finite element mesh for cylindrical specimens (green) with three inclusions at various radial offsets (red, yellow, and blue)

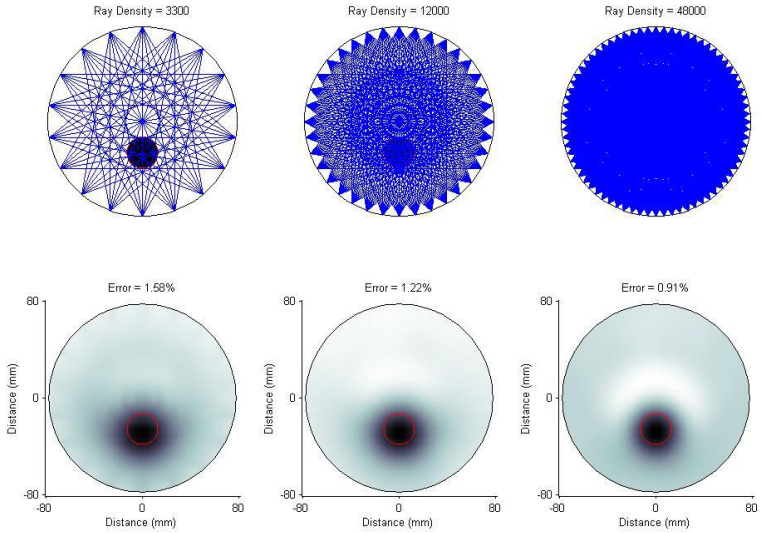

Fig. 6 Ray coverage diagrams (top) and tomograms (bottom) of PVC-void FEM data with varied ray coverage density: 20° transducer spacing (left), 10° transducer spacing (center), and 5° transducer spacing (right). The red circles in the tomograms indicate the presence of the simulated void

Fig. 6 shows the result of a series of simulated P-wave velocity tomograms of the voided PVC specimen considering different ray path configurations. In order to verify the effect of ray coverage density, the fan width was held at 60° while the transducer spacing was decreased from 20° to 5° for both models. In Fig. 6 the image error reduces as the ray density increases. As the ray density increases by a factor of approximately 4, the error in the tomogram decreases by about 0.3%. The defect indication in the reconstruction image appears to become more focused as the ray density increases. This trend is also seen when the void is located further radially from the center of the specimen. The position of the defect is correctly identified regardless of ray path density.

Fig. 7 shows the significant effect of the distribution of ray coverage on the tomographic reconstruction of the void specimen when the ray density is not changed. Clearly the local ray density varies throughout the cross-section, with zones of very high density indicated as darker rings. The maximum offset from direct transmission was increased from 40° to 80°. In order to hold the number of rays constant, the receiver spacing was held at 10° while the transmitter spacing was varied from 20° to 40°. In Fig. 7 one can see that the 60° fan width case yields the lowest error for void specimen. The 40° fan width distorts the indication toward the center, while the 80° fan width distorts it away from the center. Because of the fixed ray density, the configuration that places the most rays intersecting across the center of the void most accurately captures its location. Other results show similar behavior; for example, when the void is located closer to the center, narrow fan widths yield the greatest accuracy while when the void is located further radially from the center of the specimen, greater fan widths provide a better result. Optimally, a broad fan width would be used to capture all defects, but with a higher ray density so that all areas of the cylinder are well covered. Practically though, even the 40° fan width and 10°

transducer spacing provides reasonable result for the void specimen. Depending upon the availability of transducer arrays, testing time allowed, and automatic positioning, the highest practical ray density should be collected with a variety of angles to achieve good reconstruction results.

6. Experimental results

Although a greater number of measurements would have been desired, a limited experimental data-set was collected due to practical limitations. Air-coupled UPV data sets were collected on both the void and notch cylindrical specimens with transducer spacing of 5°. First, the transmitter and receiver locations were fixed and the specimen was rotated in 5° increments through 360°. The transmitter was then offset by 5° relative to the center of the cylinder and the specimen would be rotated again. The fan width for the PVC-void specimen was 45°, so a total of 720 UPV measurements were collected for the PVC void specimen. The fan width was increased to 60° for the notched cylindrical specimen because broader fan widths were found to significantly improve the accuracy of tomographic reconstructions when the inclusions are positioned close to the surface. This configuration gives 936 UPV measurements for the PVC notch specimen.

Because of the large velocity contrast between the air and solid, the path of the first arriving wave (P-wave) runs along the minimum distance traveled through air. Therefore it can be assumed that the wave travels from the center of the transducer to the nearest surface point on the cylinder. In other words, we assume that the incident angle with respect to the solid surface is effectively zero. The time of flight through the air gaps was subtracted from the total time so that the sources and receivers could be represented to be located on the surface of the cylinder in the reconstruction.

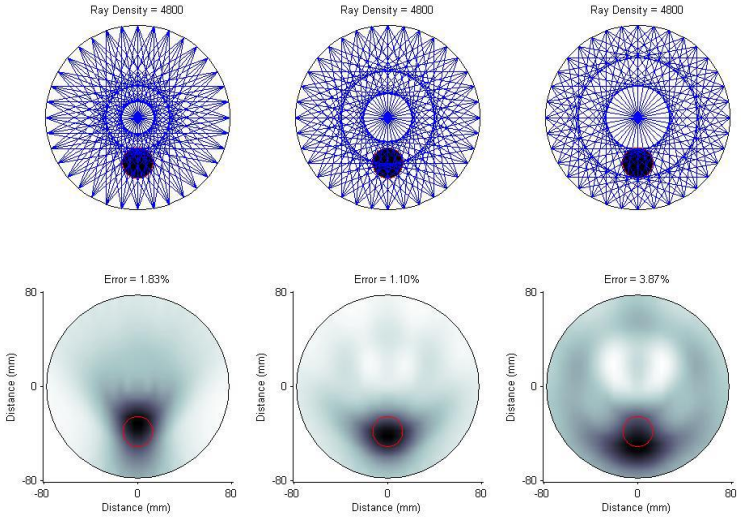

Fig. 7 Ray coverage diagrams (top) and tomograms (bottom) of PVC-void FEM data with varied ray coverage distribution: 40° fan width (left), 60° fan width (center), and 80° fan width (right). The red circles in the tomograms indicate the presence of the simulated void

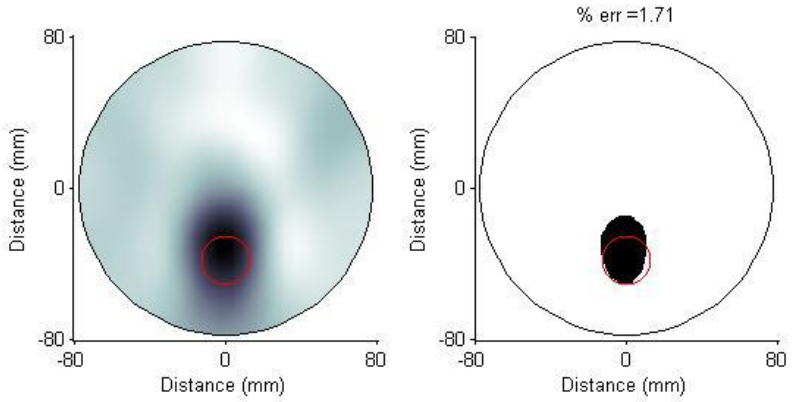

Fig. 8 Full spectrum (left) and reduced spectrum (right) tomograms of PVC-void specimen from non-contact UPV measurements

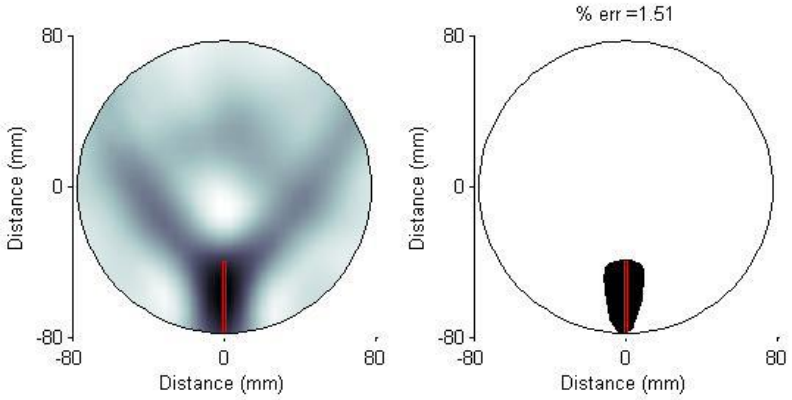

Fig. 9 Full spectrum (left) and reduced spectrum (right) tomograms of PVC-notch specimen from non-contact UPV measurements

These corrected time of flight measurements were inverted to produce the tomograms shown in Figs 8 and 9. Reduced spectrum images are also shown, where the velocity values in the bottom 25 % of the image population are shown in black and all higher velocities are shown in white. The percent error is calculated in the same manner as for the simulated tomograms so that they can be compared directly.

Fig. 8 shows the tomogram the PVC-void specimen. The error level in this tomogram is comparable to the simulated tomogram with the same ray coverage configuration. The void indication here is distorted toward the center of the cylinder. This is explained by the insufficient ray coverage nearby that inclusion. The ray density of this data set is sufficient, but the distribution

is poor since the fan width is limited to 45°. Because few of the rays pass through the inclusion at oblique angles, its location and shape are not captured perfectly. From Fig. 7 we can see that better results are expected if the fan width were increased to 60°.

Fig. 9 shows the full and reduced spectrum tomograms from the air-coupled UPV data for the PVC-notch specimen. The error of the tomogram is relatively low and the location and size of the notch are well defined by the low velocity indication. The tomographic error is low because the local ray density is high, and there are many ray paths intersecting the defect at oblique angles.

7. Conclusions

The following conclusions are drawn based on the results presented in this paper:

- The experimental study shows that useful tomograms of solid materials can be generated from air-coupled UPV measurements.
- The tomograms indicate the location and extent of the internal void and notch inclusions with reasonable accuracy.
- FEM simulations are useful to determine optimal measurement configurations and are able to predict the performance of actual UPV tomography.
- In order to minimize error in tomograms for the general case, ray density and the fan width of ray angles should be maximized.
- In order minimize error in tomograms for a specific sub-region in the sample, ray density and fan width of angles can be optimized using results of finite element analyses.

Air-coupled ultrasonic tests could lead to rapid tomography of solid objects without submerging them in fluid couplant or undergoing time consuming surface pre-preparation associated with contact measurements. With further development of the air-coupled transducers and data processing, this method could be applied to image larger cross-sections of other solids. The application of this testing configuration to concrete samples is explored in Part 2 of this paper set. Further work could also apply these methods to air-coupled tomography of rectangular sections. By implementing arrays of sensors, optimal ray coverage could be achieved more rapidly.

Acknowledgments

This work carried out in the course of research funded by the National Science Foundation through NSF project CMMI 0710777, Dr. Lawrence C. Bank program manager. The authors would like to thank Dr. Gonzalo Gallo, Dr. Michael Oelze and Dr. Marc Goueygou for their helpful suggestions concerning this work.

References

Abbaszadeh, J., Rahim, H.A., Rahim, R.A., Sarafi, S., Ayob, M.N. and Faramarzi, M. (2013), "Design procedure of ultrasonic tomography system with steel pipe conveyor", *Sensor. Actuat. A - Phys.*, **203**, 215-224.

Berriman, J., Purnell, P., Hutchins, D.A. and Neild., A. (2005), "Humidity and aggregate content correction factors for air-coupled ultrasonic evaluation of concrete", *Ultrasonics*, **43**(4), 211-217.

Cetrangolo, G.P. and Popovics, J.S. (2010), "Inspection of concrete using air-coupled ultrasonic pulse velocity", *ACI Mater. J.*, **107**(2), 155-163.

Dhital, D. and Lee, J.R. (2012), "A fully non-contact ultrasonic propagation imaging system for closed surface crack evaluation", *Exp. Mech.*, **52**(8), 1111-1122.

Gan, T.H., Hutchins, D.A. and Billson, D.R. (2002), "Preliminary studies of a novel air-coupled ultrasonic inspection system for food containers", *J. Food Eng.*, **53**(4), 315-323.

Hall, K.S. (2011), *Air-coupled ultrasonic tomographic imaging of concrete elements*, Ph.D. Dissertation, University of Illinois Urbana-Champaign, Urbana, Illinois.

Ho, K.S., Billson, D.R. and Hutchins, D.A. (2007), "Inspection of drink cans using non-contact electromagnetic acoustic transducers", *J. Food Eng.*, **80**(2), 431-444.

Jackson, M.J. and Tweeton, D.R. (1994), *Geophysical tomography using wavefront migration and fuzzy constraints*, Technical Report 9497, U.S. Bureau of Mines.

Koderu, J.P. and Rose, J.L. (2013), "Mode controlled guided wave tomography using annular array transducers for SHM of water loaded plate like structures", *Smart Mater. Struct.*, **22**, 125021.

Naik, T.R., Malhotra, V.M. and Popovics, J.S. (2004), "The ultrasonic pulse velocity method", in *CRC Handbook on Nondestructive Testing of Concrete*, 2nd Ed., (Eds., V.M. Malhotra and N.J. Carino), CRC Press, Boca Raton, Chapter 8.

Radon, J. (1917), "Uber die bestimmung von funktionnen durch ihre integralwerte lngs gewisser mannigfaltikeiten", *Berichte uber die Verhandlungen der Sschsischen Akademie der Wissenschaften zu Leipzig, Mathematisch-Naturwissenschaftliche Klasse*, **69**, 262-277.

Sanabria, S.J., Mueller, C., Neuenschwander, J., Niemz, P. and Sennhauser, U. (2011), "Air-coupled ultrasound as an accurate and reproducible method for bonding assessment of glued timber", *Wood Sci. Technol.*, **45**(4), 645-659.

Wright, W.M.D., Hutchins, D.A., Gachagan, A. and Hayward, G. (1996), "Polymer composite material characterization using a laser/air-transducer system", *Ultrasonics*, **34**(8), 825-833.